Journal of Alloys and Compounds 509 (2011) 6395–6399

Contents lists available at ScienceDirect

Journal of Alloys and Compounds

journal homepage: www.elsevier.com/locate/jallcom

Solid-state synthesis and spark plasma sintering of $SrZrO_3$ ceramics

B. Popescu*, S. Enache, C. Ghica, M. Valeanu

National Institute of Materials Physics, 105 bis Atomistilor Str., PO Box MG 7, 077125 Bucharest, Romania

ARTICLE INFO

Article history:
Received 2 November 2010
Received in revised form 28 February 2011
Accepted 2 March 2011
Available online 10 March 2011

Keywords:
Ceramics
Solid state reaction
Sintering
Microstructure

ABSTRACT

$SrZrO_3$ powders are obtained by solid state reaction from $SrCO_3$ and ZrO_2 precursors, without involving intermediate calcination and grinding steps. The resulted powders are essentially within a single phase, with sub-micron average crystallite size. Pellets of these powders show a relatively poor sintering behavior, when fired up to 1600 °C. Alternatively, spark plasma sintering technique is used in order to obtain nearly 100% dense samples at the expense of excessive grain coarsening (i.e., up to 5 μm in diameter). Crystalline structure, composition and morphology of the specimens obtained in this work are investigated by X-ray diffraction, scanning and transmission electron microscopy together with energy dispersive X-ray spectroscopy.

1. Introduction

Strontium zirconate ($SrZrO_3$) belongs to the perovskite family and has an orthorhombic structure at room temperature, with space group *Pbnm* [1,2]. Acceptor doped $SrZrO_3$ perovskite oxides have been studied for their high-temperature proton conductivity [3], which makes them potential candidates for electrolytes in novel electrochemical devices such as solid oxide fuel cells and hydrogen sensors. Due to its high dielectric constant, high breakdown strength and low leakage current density [4,5], $SrZrO_3$ has been extensively investigated as a possible candidate material for high-k gate dielectrics (i.e., E_g = 5.6 eV) [6].

Recently, due to their simple structure and compatibility with metal oxide semiconductor technologies [7], $SrZrO_3$ has been studied as a potential candidate material for the next generation of nonvolatile information storage purposes [8,9]. For instance, random access memories (RAMs) based on thin films of $SrZrO_3$ would present excellent resistive switching properties such as low opearating voltage, fast switching, high resistance ratio and good stability, improved endurance and retention time [10,11]. The possibility to cast thin films of $SrZrO_3$ offers the opportunity not only to study in detail the intrinsic mechanisms responsible for the resistive switching processes, but also to improve the functional parameters, such as the switching life-time by controlling Zr-deficiency [12].

$SrZrO_3$ (SZO) powders were initially obtained by solid-state reaction of $SrCO_3$ and ZrO_2 at 1473 K for 48 h, with intermittent grinding [13,14]. The resulted powders were inhomogeneous and coarse, with nonuniform size distribution. In order to avoid that, wet chemical methods such as sol–gel [15], co-precipitation [16] and hydrothermal methods [17] have been employed to synthesize SZO powders with desired stoichiometry. However, several disadvantages have been noted with these techniques such as the evaporation of solvents resulting in phase segregation and the alteration of stoichiometry due to incomplete precipitation, expensive chemicals and time consuming processes.

Alternatively, auto-ignition (combustion) of a precursor solution containing metal ions, oxidant, and a fuel leads to fine crystalline powders (~15 to 25 nm) [18]. Pellets of these powders show good sintering behavior, with relative density values >98% of the theoretical one, (i.e., 5.46 g/cm^3, from Refs. [1,2]) when heated at 1470 °C for 4 h. It turns out that, nevertheless, the combustion method demands an elaborate preparation procedure and involves corrections for the oxidant-to-fuel ratio and for the pH of solution. It is, however, worth it to mention that the combustion method leads to single phase SZO powders, without making use of intermediate calcination and grinding steps.

In this work, we show that SZO powders can be readily obtained by solid state reaction from $SrCO_3$ and ZrO_2 precursors, without involving intermediate calcination and grinding steps. The synthesis time is reduced, from 48 to 8 h [13]. The resulted powders are essentially within a single phase (i.e., with orthorhombic *Pbnm* crystal symmetry). They have a relatively wide distribution of grain size, with the average value of ~385 nm. Pellets of these powders exhibit a relatively poor sintering behavior, with a relative density up to ~92% of the theoretical one, when fired in air at 1600 °C for 5 h. Alternatively, in order to improve that, we make use of spark-plasma sintering (SPS) technique. SPS gained much attention lately because of the rapid heating, the enhanced densification rate, and the improved microstructure [19,20]. The crystalline structure

* Corresponding author. Tel.: +40 213690185; fax: +40 213690177.
E-mail address: bogdan@infim.ro (B. Popescu).

0925-8388/$ – see front matter © 2011 Elsevier B.V. All rights reserved.
doi:10.1016/j.jallcom.2011.03.009

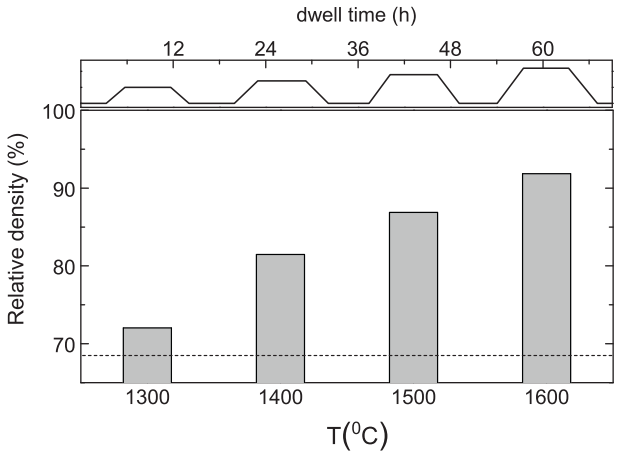

Fig. 1. Relative densities of *one* SZO pellet sintered successively for 5 h at the indicated temperatures, with a heating/cooling rate of 5 °C/min. The relative density of the *green* pellet (i.e., ∼69.7%) is given by the dashed line. The upper graph shows the heat treatment history.

and morphology of *green* powders and dense pellets are analyzed by X-ray diffraction (XRD), scanning and transmission electron microscopy (SEM/TEM), whereas the stoichiometry is verified by energy-dispersive X-ray spectroscopy (EDS).

2. Experimental

$SrZrO_3$ powders are obtained by conventional solid-state reaction. For that, equimolar quantities of $SrCO_3$ (i.e., aged powder stored in glass vial) and ZrO_2 (i.e., from Merck, with >98.5% purity and <2.5 wt.% of HfO_2) were mixed and ground thoroughly in agate mortar using alcohol as lubricant (C_2H_5OH, with >96% purity from Chimopar SA). The powder was then let to dry out and placed in alumina (Al_2O_3) crucibles, moved to furnace and fired in air at 1250 °C for 8 h, with a heating/cooling rate of 3 °C/min.

Differential scanning calorimetry (DSC) and thermo-gravimetric (TG) measurements are carried out on precursors and their equimolar mixture. For that, we make use of a modular Thermogravimetric Analyzer TGA (Evolution SETARAM) that allows to measure the heat flow and the mass loss simultaneously, upon heat treatment and under specific conditions (i.e., 1 bar air). The precursors are studied separately. The DSC/TG curves are recorded up to 1500 °C, with a temperature sweep rate of 10 °C/min. From that, the decomposition temperatures (e.g., for $SrCO_3$) and phase transformations (e.g., ZrO_2) are determined, respectively. The equimolar mixture of precursors is, however, subjected to a different heat treatment profile which mimics in great detail the one used in this work for powder synthesis. Explicitly, the DSC/TG curves are measured up to the temperature of formation of SZO (i.e., ∼1250 °C), with a temperature sweep rate is 3 °C/min. At 1250 °C, the temperature is kept constant for 8 h and the heat flow and mass loss are continuously monitored.

Crystalline structure of as-prepared powders and sintered pellets are examined by X-ray diffraction (XRD) technique using a X-ray diffractometer (Bruker D-8 Advance) with rotating Nickel filtered Cu anode and silicon strip detector (Lynx-Eye). $\theta - 2\theta$ scans are performed in Bragg–Brentano geometry between $2\theta = 20°$ and 75°, with a speed of 4°/min. The XRD peaks are indexed by using the Inorganic Crystal Structure Database (ICSD). Lattice constants are determined from fit to the corresponding XRD spectra by using the Material Analysis Using Diffraction (MAUD) software.

Morphology of *green* powders and sintered pellets is studied by using a Zeiss Evo 50 XVP scanning electron microscope (SEM) with LaB_6 cathode enabling 2 nm resolution. For that, the powder is dispersed in distilled water by using a ultrasonic-bath for 15 min. Sintered pellets are cut transversally and polished with diamond paste, down to a granulation of 0.5 μm. Subsequently, in order to reveal the intergrain microstructure, the sintered specimens are thermally etched for 1/2 h at a temperature with 50 °C below the sintering temperature (i.e., at 1500 °C).

The microstructure and stoichiometry of as-prepared powders are analyzed by transmission electron microscopy (TEM) by using a JEOL 200 CX electron microscope operated at 200 kV and equipped with an IXRF EDS unit. Additionally, one sintered pellet (i.e., at 1600 °C for 5 h) was ground in a mortar and dispersed on holey membrane TEM grids by using ethylic alcohol.

Classical sintering (CS) is carried out in a Nabertherm furnace (LHT 04/18). For that, *one* pellet with a diameter of 16 mm is made out of ∼3.5 g of powder by uniaxial pressing at ∼350 MPa. The relative density of the resulted pellet is ∼69.3% of the theoretical one. The pellet is then sintered successively for 5 h at the temperatures shown in Fig. 1, with a heating/cooling rate of 5 °C/min. After each sintering cycle, the geometrical density is determined. During the sintering processes, the *overall* mass loss was less than ∼0.7%.

Spark-plasma sintering (SPS) is conducted by using a FCT Systeme (GmbH HP D 5/2) furnace in conjunction with two Poisson pistons that can press with a force up to 50 kN on a 20 mm diameter graphite die. For that, ∼4.0 g of powder is poured in the graphite die and pre-pressed uniaxially (i.e., at 25 MPa) at room temperature. Subsequently, the die is moved to the SPS system and pressed with a constant force of 20 kN upon the heating process. In order to avoid sample embrittlement, the force is released prior the cooling process. An estimate for the relative green density is ∼70.2%. The system is evacuated to a pressure of 40 Pa and the temperature is increased up to 1550 °C, with a rate of 150 °C/min. At maximum temperature (i.e., at 1550 °C), the output power is manually adjusted in order to increase densification rate. A hint to that is the rapid change in the relative distance between the pistons which, for our sample, occurs above 1430 °C. The temperature is measured by using an optical pyrometer focused on the external surface of the die. The heating is provided by a pulsed *dc* current that is allowed to pass through the conductive die which acts as heating element. The heating pattern consists of 14 pulses (i.e., 12:2/ON:OFF pulses). The pulse period is 3 ms. The total time of one sequence (cycle) is 0.04 s. The operating voltage and the peak current were 5 V and 1600 A, respectively. After the experiment is complete, the pressure is released, the power is switched off and the sample is let to cool to room temperature, with a rate ∼400 °C/min.

3. Results and discussion

DSC and TG measurements performed on precursors show that $SrCO_3$ exhibits the polymorphic transformation from the orthorhombic phase (space group P*mcn*) to the rhombohedral phase (space group R-3*m*) [21] at 932 °C, whereas the decomposition reaction occurs at 1153 °C. These features are accompanied by up to ∼45% mass loss that is due to CO_2 emission from $SrCO_3$ decomposition, mainly. ZrO_2 shows the phase transformations from monoclinic (i.e., low temperature phase) to tetragonal (i.e., high temperature phase) at 1196 °C and the reversible martensitic transformation, at 1017 °C [22].

The DSC/TG curves measured on the equimolar mixture following the heat treatment profile used in this work (i.e., 1250 °C for 8 h, with a heating rate of 3 °C/min) shows the phase transformations observed for precursors, with the following differences: (i) the decomposition temperature of $SrCO_3$ is lower (i.e., 1033 °C) due to the presence of acidic ZrO_2 in the mixture; (ii) the phase transformation from monoclinic to tetragonal occurs at a higher temperature (i.e., at 1210 °C). The formation of $SrZrO_3$ is observed at 1236 °C. The exoenergetic peak corresponding to the reversible transformation of ZrO_2 from tetragonal to monoclinic is not present upon cooling to room temperature. This indicates that $SrZrO_3$ forms readily from SrO and tetragonal ZrO_2.

The fact that the features corresponding to the reversible transformation of ZrO_2 (i.e., from tetragonal to monoclinic phase) are not present in the equimolar mixture indicates that the formation of SZO powders is complete after 8 h (i.e., or longer) of thermal treatment at 1250 °C. Shorter dwell time results in incomplete reacted specimens; i.e., in the DSC curve, the features corresponding to the reversible phase transformation of precursors i.e., ZrO_2) are present upon cooling to room temperature.

3.1. As prepared powders

Fig. 2 shows the XRD pattern of as-prepared powders. Together with that, the XRD spectra measured on sintered pellets (CS and SPS) are shown. All specimens exhibit the Bragg reflections corresponding to the orthorhombic phase (i.e., with *Pbnm* crystal symmetry, from Refs. [1,2]). Thus, no structural changes are observed in the heated samples when compared to as-prepared powders. This indicates that the formation of $SrZrO_3$ phase is essentially complete during the solid-state reaction process itself, without involving intermediate calcination and grinding steps. It is, nevertheless, worth it to point out that the diffraction peak at $2\theta = 28.17°$ corresponding to some unreacted monoclinic ZrO_2 phase is observed in *all* XRD patterns. However, the contribution of

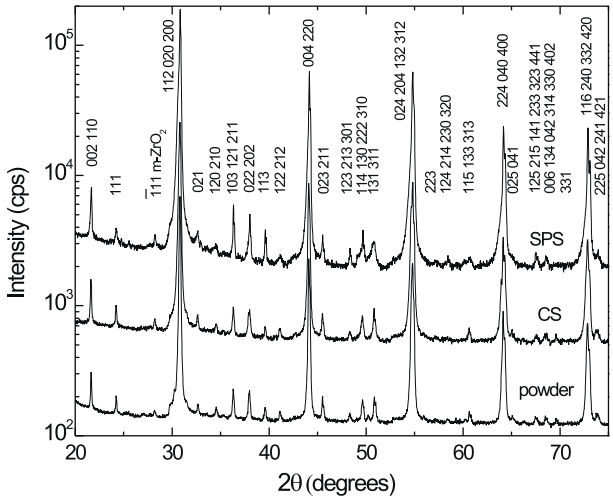

Fig. 2. XRD patterns of $SrZrO_3$ powders obtained by solid state reaction at 1250 °C for 8 h, without involving intermediate calcination and grinding steps. Together with that, the XRD spectra measured on sintered pellets (classical and SPS) are shown. Except for the main ($\bar{1}11$) Bragg reflection of monoclinic ZrO_2 at 28.17°, all the intensity peaks correspond to SZO with orthorhombic *Pbnm* crystal symmetry.

the ZrO_2 phase to the XRD spectra estimated from fit to data is less than 0.36 wt.% for *all* specimens.

The lattice constants determined from fit to the corresponding XRD data are slightly different (i.e., $a = 0.5801$ nm, $b = 0.5816$ nm and $c = 0.8207$ nm) than those reported so far [1,2]. The average crystallite size of green powders is ~385 nm. This value is in reasonable agreement with that observed in SEM micrographs (i.e., in Fig. 3a).

In Fig. 4(b), TEM images obtained for green powders show a wide dispersion of grain size, from tens of nm up to several hundreds of nm or 1 μm. Fig. 4a – right side shows the diffraction pattern from a large selected area, which includes small and large crystal grains. The diffraction pattern shows a large number of diffuse and streaked diffraction spots and rings, which results from small grain size and, eventually, heavily faulted crystals. The Miller indices corresponding to the main reflections for the orthorhombic $SrZrO_3$ phase [1,2] are indicated. The broadening and splitting of the diffraction rings might be related to a small unit cell distortion. The inset in Fig. 4b shows a large faulted $SrZrO_3$ crystal grain. The diffraction contrast indicates the presence of planar defects and, possibly, twin domains. The EDS quantitative analysis indicates that Sr and Zr are present in equal atomic concentrations, according to the $SrZrO_3$ stoichiometry.

3.2. Classical sintering

Classical sintering (CS) yields to poorly dense pellets (i.e., ~91.9%, when treated up to 1600 °C for 5 h). However, from the data in Fig. 1, one may point out that densification already starts upon heat treatment at 1300 °C. Nevertheless, the values for the relative densities in Fig. 1 do not flatten off with increasing temperature. This suggests that neither the temperature nor the dwell time where optimally chosen in order to obtain highly dense pellets (i.e., with relative densities >98%).

In Fig. 3b, the SEM micrographs taken on CS pellets reveal conglomerates of sub-micron-size grains delineated by a network of micro-fractures. This may result from the processing route used in this work that combines (i) the nonuniform stress distribution along the pellets resulted from uniaxial pressing, (ii) the wide grain size distribution and (iii) the lack of grinding steps, which leads to relatively large conglomerates in the green powders (i.e., as shown in Fig. 3a). The presence of micro-fractures indicates that, to some

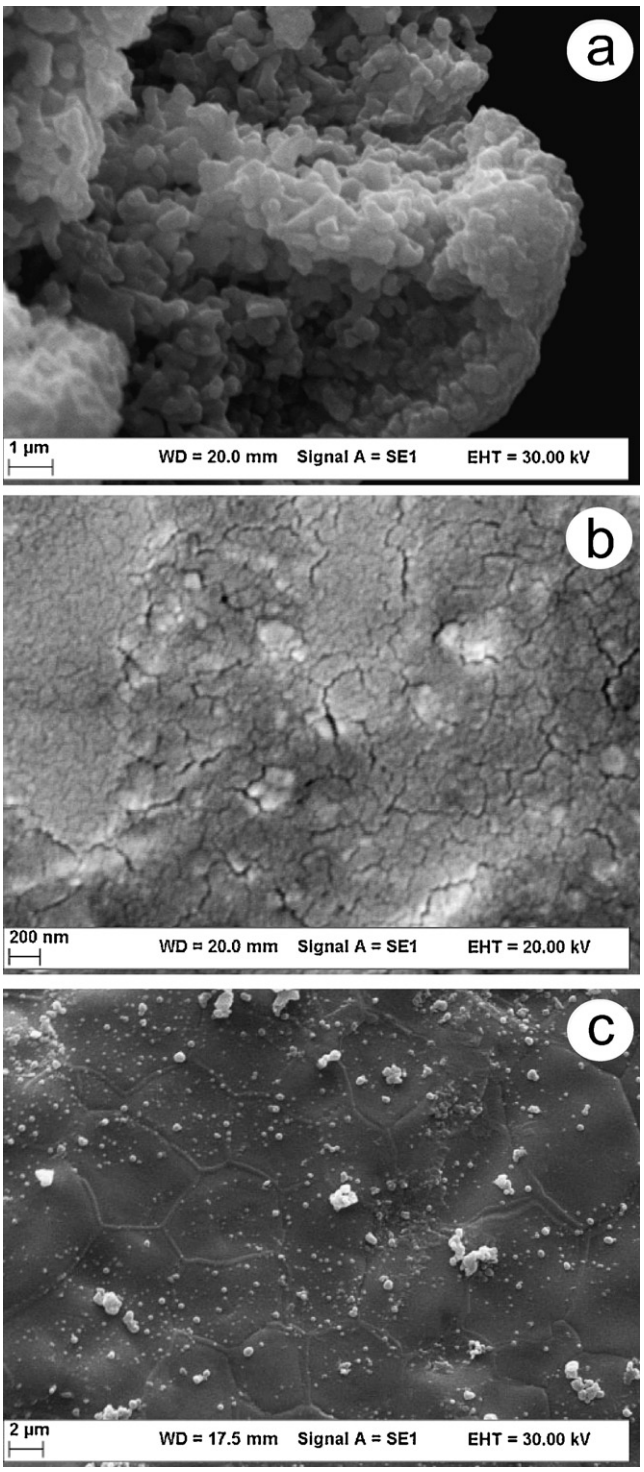

Fig. 3. SEM micrographs of $SrZrO_3$ powders obtained by solid-state reaction at 1250 °C for 8 h (i.e., in (a)). In (b) and (c), microstructure of transversal cuts through SZO pellets sintered classically and by SPS technique are shown, respectively.

extent, the values for the geometrical density for the CS pellet are somewhat underestimated. However, in order to verify the influence of the classical sintering route used in this work on the density values in Fig. 1, we have prepared a pellet in similar condition and fired it for 5 h at 1600 °C *only*, with a heating/cooling rate of 5 °C/min. The value for the geometrical density was ~91.1% of the theoretical one whereas a relative value of ~94.5% is obtained by using Archimedes's method.

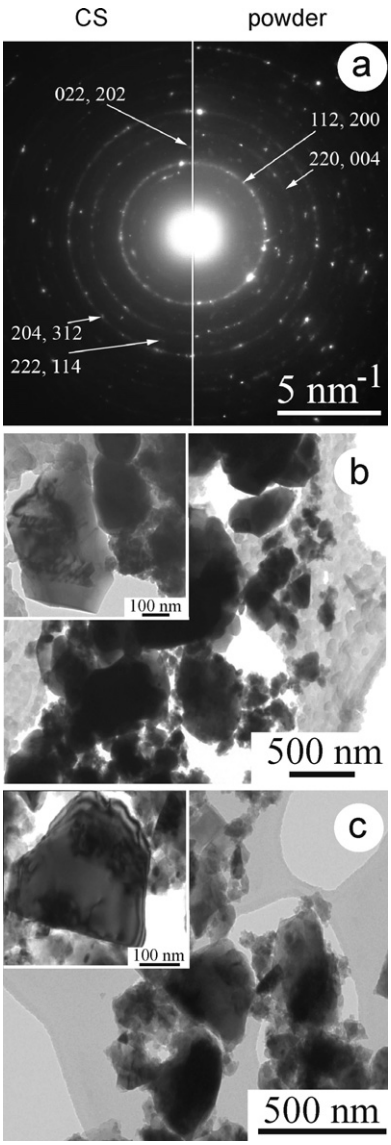

Fig. 4. Small magnification TEM images of SZO powder samples. In (a), the diffraction patterns for green powders (right side) and the ground CS pellet (left side) are presented together for comparison. In (b) and (c), TEM micrographs for the green powders and for the ground CS pellet are shown, respectively. The insets show SZO crystal grains with multiple structural defects.

TEM micrographs of ground CS pellets are shown in Fig. 4c. The image is similar to that obtained for green powders shown in Fig. 4b. The grains have a wide size distribution, from tens up to hundreds of nm. Larger grains contain extended structural defects such as dislocations and planar defects (i.e., see the inset in Fig. 4c). The diffraction pattern in Fig. 4a – left side, confirms the orthorhombic $SrZrO_3$ phase observed in as-prepared powders, with the slight difference that in this case the diffraction spots do not show a diffuse aspect. EDS analysis indicates that stoichiometry is preserved.

3.3. Spark plasma sintering

The formation of micro-fractures in CS pellets can be avoided by making use of SPS technique. Apart from spark impact pressure, Joule heating and electrical field induced diffusion effect, the advantage of the SPS technique over the CS one is the continuous uniaxial pressing used in the former that forces the voids out of the sample via grain boundaries. The heating rate and dwell time can be adjusted so as highly dense samples are obtained, without a major change in grain-size. However, in our SPS experiment, we have deliberately subjected the sample to prolonged heat treatment at 1550 °C, for two reasons: (i) to assure that a highly dense pellet is obtained since the only parameter to monitor that is the relative change of piston positions and (ii) to overcome the temperature gradients within the sample, which results from the nonuniform distribution of current density along the constitutive grains. The relative density – as determined by Archimedes's method, of the spark-plasma sintered sample is over 96% of the theoretical value. In Fig. 3c, the SEM micrograph on a fractured SPS sample shows excessive grain coarsening (i.e., up to 5 μm in diameter). The sample does not show pores or micro-fractures (i.e., similar to those in Fig. 3b for CS samples), even at larger scale (i.e., up to hundreds of μm). This suggests that the sintering process was effective, leading to specimens with densities near the ideal value (i.e., 100%). The different density values from above might be due to sample embrittlement upon the cooling process, which combines fast pressure release with high temperature sweep rates (i.e., 400 °C/min). This may result in major cracks/voids within the sample. It is, nevertheless, worth it to mention that the grain boundaries in the SPS sample exhibit a well defined geometry (i.e., ∼200 nm in width). Their composition is similar to that observed in the adjacent grains (i.e., stoichiometric SZO, from EDS). From this point of view, it may be meaningful to discern on whether the grain boundaries exhibit crystalline structure or not since the morphology of grain boundaries is often related to a drop of ionic conductivity.

4. Conclusions

Single phase $SrZrO_3$ powders are obtained by solid state reaction from $SrCO_3$ and ZrO_2 precursors, without involving intermediate calcination and grinding steps. The time for powder synthesis was reduced, from 48 to 8 h. The resulted powders consist of sub-micron grains with a wide distribution in size, from tens to hundreds of nm.

SZO forms readily from SrO and tetragonal ZrO_2. To promote the formation of SZO, it is essential to dwell above the temperature corresponding to the martensitic transformation of ZrO_2, from the high temperature phase (i.e., above 1210 °C) to the low temperature one (i.e., below 1017 °C). This feature suggests that the synthesis temperature may be further reduced in order to obtain SZO powders with smaller and narrower distribution of grain size.

Classical sintering yields to poorly dense specimens, when fired at 1600 °C for 5 h (i.e., with relative density of ∼92%). They consist of sub-micron grains delineated by a network of micro-fractures that most probably results from the preparation route used in this work. Alternatively, SPS technique leads to highly dense specimens which are morphologically different than those prepared by classical sintering route; i.e., the SPS sample shows excessive grain coarsening (i.e., up to 5 μm in diam.) due to prolonged heat treatment. The grain boundaries of SPS sample are substituted for nm-size domains with well defined geometry (i.e., ∼200 nm wide) and stoichiometry. To some extent, one would expect some contribution of these domains to the overall electronic transport properties of SPS samples since the morphology of grain boundaries is often related to a drop of ionic conductivity.

Acknowledgments

The authors thank A.D. Crisan for XRD measurements, I. Enculescu for assistance with the SEM facility, I. Anton for preparation of the TEM specimens and C. Valsangiacom for DSC/TG measurements. This work was supported by the Romanian Ministry of Education and Research.

References

[1] A. Ahtee, M. Ahtee, A.M. Glazer, A.W. Hewat, Acta Crystallogr. 32 (1976) 3243–3246.
[2] R. Ubic, G. Subodh, J. Alloys Compd. 488 (2009) 374–379.
[3] T. Omata, T. Fuke, S. Otsuka-Yao-Matsuo, Solid State Ionics 179 (2008) 1116–1119.
[4] C.H. Chen, W. Zhu, T. Yu, X.F. Chen, X. Yao, Appl. Surf. Sci. 211 (2003) 244.
[5] H.-Q. Ling, A.-D. Li, D. Wu, Y.-F. Tang, Z.-G. Liu, N.-B. Ming, Mater. Chem. Phys. 75 (2002) 170.
[6] Y.S. Lee, J.S. Lee, T.W. Noh, D.Y. Byun, K.S. Yoo, K. Yamaura, E.T. Muromachi, Phys. Rev. B 67 (2003) 113101.
[7] R. Waser, M. Aono, Nat. Mater. 6 (2007) 833.
[8] Y. Wang, Z. Wang, H. Xu, D. Li, J. Alloys Compd. 484 (2009) 230–232.
[9] Y.-T. Chen, J.-Y. Tseng, S.-R. Jian, H.-G. Chen, S.-U. Jen, J. Alloys Compd. 485 (2009) 822–825.
[10] M.-H. Lin, M.-C. Wu, C.-H. Lin, T.-Y. Tseng, J. Appl. Phys. 107 (2010) 124117.
[11] M.-H. Lin, M.-C. Wu, C.-Y. Huang, C.-H. Lin, T.-Y. Tseng, J. Phys. D: Appl. Phys. 43 (2010) 295404.
[12] J. Wu, Z. Wen, Di Wu, H. Zhai, A. Li, J. Alloys Compd. 509 (2011) 2050–2053.
[13] E.K. Keler, A.K. Kuzestor, Zh. Prikl Khim. 34 (1961) 2146.
[14] J. Huang, L. Zhou, Z. Wang, Y. Lan, Z. Tong, F. Gong, J. Sun, L. Li, J. Alloys Compd. 487 (2009) L5–L7.
[15] C.-Y. Liu, T.-Y. Tseng, J. Phys. D: Appl. Phys. 40 (2007) 2157.
[16] H.S. Potdar, S.B. Deshpande, A.J. Patil, A.S. Deshpande, Y.B. Khollam, S.K. Date, Mater. Chem. Phys. 65 (2000) 178.
[17] M.M. Lencka, E. Nielsen, A. Anderko, R.E. Riman, Chem. Mater. 9 (1997) 1116.
[18] J.K. Thomas, H. Padma Kumar, R. Pazhani, S. Solomon, R. Jose, J. Koshy, Mater. Lett. 61 (2007) 1592.
[19] X. Wan, A. Hu, M. Li, C. Chang, D. Mao, J. Mater. Charact. 59 (2008) 256.
[20] W. Luan, L. Gao, H. Kawaoka, T. Sekino, K. Niihara, Ceram. Int. 30 (2004) 405.
[21] R.C. Evans, An Introduction to Crystal Chemistry, Cambridge University Press, Cambridge, UK, 1966, p. 410.
[22] B. Basu, Int. Mater. Rev. 50 (2005) 239–256.